(Received 14 April 2024, Accepted 8 July 2024, Scheduled 17 July 2024)

A Novel Three-Coil WPT System with Automatic CC-CV Transition Function

Xuebin Zhou[1,*], Yilin Wang[2], Yuhang Jiang[2], and Lin Yang[2]

[1] College of Intelligent Manufacturing, Hunan University of Science and Engineering, China
[2] College of Electronic and Electrical Engineering, Henan Normal University, China

ABSTRACT: In order to prolong the service life of lithium batteries, the charging process is usually divided into two stages: first constant current (CC) charging and then constant voltage (CV) charging. This letter proposes a three-coil structure wireless power transfer (WPT) system to realize inherent CC and CV characteristics and automatic CC-CV transition function. During charging, the proposed system can operate in S-S-LCC tank for CC charging and in S-S-S tank for CV charging, respectively. Different from the previous closed-loop control, hybrid topology switching and dual-frequency switching methods, the proposed method has automatic CC-CV transition function due to the special circuit structure. Therefore, the communication links, state-of-charge detection circuits, and open-circuit protection circuits are omitted, which ensures the high reliability and low cost of the system. Finally, a verification experimental prototype with a rated power of 480 W is built to verify the feasibility of the proposed system.

1. INTRODUCTION

The charging method of constant current (CC) and then constant voltage (CV) can ensure the high efficiency of charging and prolong the life of the battery. The three closed-loop control methods of phase shift control [1], frequency conversion control [2], and DC-DC converter control [3] are currently commonly used technologies to realize CC and CV outputs. However, all three methods have disadvantages. Phase shift control is difficult to achieve zero-voltage switching when the load changes greatly, resulting in increased inverter loss. There is a possibility of frequency bifurcation in the frequency conversion control technology, which affects the stability of the system, and it is difficult to achieve zero phase angle (ZPA) operation, resulting in reactive power circulation in the system and increased losses. DC-DC auxiliary control technology has a large number of components, high cost, and high system complexity.

The hybrid topology switching method realizes the conversion of the system's CC and CV outputs by controlling the on-off of the switches [4–6]. However, it introduces additional AC switches, corresponding drive circuits and passive components in the system, which increases the complexity of the circuit structure.

Dual-frequency switching method is also a commonly used method to realize CC and CV outputs [7–9]. However, this method is not only difficult to design the parameters of the compensation components, but also difficult to limit the CC and CV frequencies within the frequency range specified by the standard.

In order to optimize the existing CC and CV wireless power transfer (WPT) systems, this letter proposes a three-coil WPT system, which can not only realize CC and CV outputs but also automatically complete the transition from CC to CV mode. Compared with the previous closed-loop control, hybrid topology switching and dual-frequency switching methods, the proposed method does not require communication links, state-of-charge detection circuits, and open-circuit protection circuits. Therefore, high reliability, simple structure, and low cost can be ensured in the proposed system. It is worth noting that, similar to the above-mentioned hybrid topology switching and dual-frequency switching methods, the proposed method is suitable for scenarios with fixed mutual inductance, such as electric bicycle charging applications.

2. SYSTEM STRUCTURE AND THEORETICAL ANALYSIS

2.1. System Structure

The architecture diagram of the proposed three-coil WPT system is shown in Fig. 1, which is also the circuit diagram of the system working in the CC mode. U_D is the DC input voltage, and four Metal-Oxide-Semiconductor Field Effect Transistors (MOSFETs) (Q_1, Q_2, Q_3, and Q_4) form an inverter to provide AC power to the system. L_1, L_2, and L_3 are coils forming a three-coil loosely coupled transformer. C_1, C_2, C_3, and C_4 are the compensation capacitors of the primary, relay, and secondary circuits, respectively. L_4 is the secondary side compensation inductance. M_{12}, M_{13}, and M_{23} are the mutual inductances. R_1, R_2, and R_3 are the parasitic resistances of L_1, L_2, and L_3, respectively.

* Corresponding author: Xuebin Zhou (zhouxuebin821025@huse.edu.cn).

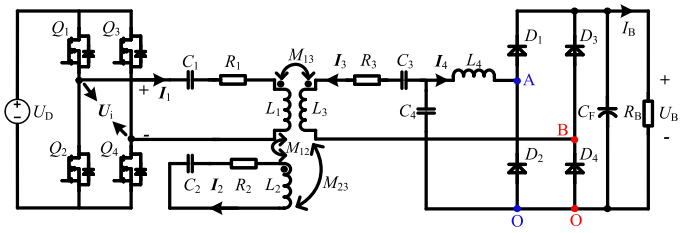

FIGURE 1. The architecture diagram of the proposed three-coil WPT system.

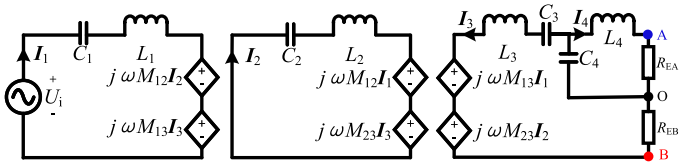

FIGURE 2. Simplified circuit diagram in CC mode.

2.2. CC Mode

In the initial stage of charging, due to the small battery resistance, the battery voltage is less than the voltage across C_4. At this time, diodes D_1, D_2, D_3, and D_4 are conductive, and the system performs CC charging with a special S-S-LCC structure. The simplified circuit of the proposed topology under the CC mode is shown in Fig. 2. R_{EA} and R_{EB} are the equivalent resistance between terminals A, O and terminals B, O, respectively. Since two half-bridge rectifiers are connected in parallel, the following equation can be obtained as

$$\begin{cases} U_{AO} = U_{BO} \\ \frac{1}{R_{EA}} + \frac{1}{R_{EB}} = \frac{\pi^2}{2R_B} \end{cases} \tag{1}$$

According to Kirchhoff's voltage law (KVL) and Fig. 2, Equation (2) can be obtained.

$$\begin{cases} \mathbf{U}_i = \left(\frac{1}{j\omega C_1} + j\omega L_1\right)\mathbf{I}_1 + j\omega M_{12}\mathbf{I}_2 + j\omega M_{13}\mathbf{I}_3 \\ 0 = \left(\frac{1}{j\omega C_2} + j\omega L_2\right)\mathbf{I}_2 + j\omega M_{12}\mathbf{I}_1 + j\omega M_{23}\mathbf{I}_3 \\ 0 = \left(\frac{1}{j\omega C_4} + j\omega L_4 + R_{EA}\right)\mathbf{I}_4 + \frac{1}{j\omega C_4}\mathbf{I}_3 \\ 0 = \left(R_{EB} + j\omega L_3 + \frac{1}{j\omega C_4} + \frac{1}{j\omega C_3}\right)\mathbf{I}_3 + j\omega M_{13}\mathbf{I}_1 \\ \quad + j\omega M_{23}\mathbf{I}_2 + \frac{1}{j\omega C_4}\mathbf{I}_4 \end{cases} \tag{2}$$

To simplify the analysis process, it is assumed that the system satisfies the following resonance conditions.

$$\begin{cases} \omega^2 L_1 C_1 = \omega^2 L_2 C_2 = \omega^2 L_4 C_4 = 1 \\ \frac{1}{\omega C_4} + \frac{1}{\omega C_3} - \omega L_3 = \frac{-2\omega M_{13} M_{23}}{M_{12}} \end{cases} \tag{3}$$

Substituting (1), (3) into (2), Equation (4) can be deduced.

$$\begin{cases} \mathbf{I}_3 = \frac{-2R_B M_{23}\mathbf{U}_i}{\pi^2\omega^2 L_4^2 M_{12}} \\ \mathbf{I}_4 = \frac{\left(\pi^2\omega L_4 - 2R_B\right)M_{23}\mathbf{U}_i}{\pi^2\omega^2 L_4^2 M_{12}} \\ Z_{\text{in}} = \frac{\mathbf{U}_i}{\mathbf{I}_1} = \frac{\pi^2\omega^2 {L_4}^2 M_{12}^2}{2M_{23}^2 R_B} \end{cases} \tag{4}$$

From (4), the root mean square (RMS) value of the equivalent input current I_O of the rectifier can be derived as

$$I_O = I_3 + I_4 = \frac{M_{23}U_i}{\omega L_4 M_{12}} \tag{5}$$

According to $U_i = \frac{2\sqrt{2}}{\pi}U_D$ and $I_O = \frac{\pi}{2\sqrt{2}}I_B$, the charging current I_B can be obtained as

$$I_B = \frac{4}{\pi^2}\frac{M_{23}U_D}{\omega L_4 M_{12}} \tag{6}$$

Through (4) and (6), it can be found that the system can realize load-independent CC output and zero phase angle (ZPA) operation.

2.3. CV Mode

As charging progresses, the battery voltage continues to increase. When the battery voltage is higher than the voltage across C_4, the diodes D_1 and D_2 are forced to reverse bias, making the branch where L_4 is located open circuit. Consequently, the system automatically converts to the S-S-S structure to perform CV charging. The system structure and simplified circuit diagram in CV mode are shown in Figs. 3(a) and (b). According to KVL, Equation (7) can be obtained.

$$\begin{cases} \mathbf{U}_i = \left(\frac{1}{j\omega C_1} + j\omega L_1\right)\mathbf{I}_1 + j\omega M_{12}\mathbf{I}_2 + j\omega M_{13}\mathbf{I}_3 \\ 0 = \left(\frac{1}{j\omega C_2} + j\omega L_2\right)\mathbf{I}_2 + j\omega M_{12}\mathbf{I}_1 + j\omega M_{23}\mathbf{I}_3 \\ 0 = j\omega M_{13}\mathbf{I}_1 + j\omega M_{23}\mathbf{I}_2 \\ \quad + \left(R_{EB} + j\omega L_3 + \frac{1}{j\omega C_4} + \frac{1}{j\omega C_3}\right)\mathbf{I}_3 \end{cases} \tag{7}$$

Substituting (3) into (7), Equation (8) can be derived as

$$\begin{cases} \mathbf{U}_{BO} = \mathbf{I}_3 R_{EB} = \frac{M_{23}\mathbf{U}_i}{M_{12}} \\ Z_{\text{in}} = \frac{\mathbf{U}_i}{\mathbf{I}_1} = \frac{M_{12}^2 R_{EB}}{M_{23}^2} \end{cases} \tag{8}$$

According to $U_i = \frac{2\sqrt{2}}{\pi}U_D$ and $U_{BO} = \frac{\sqrt{2}}{\pi}U_B$, the charging voltage U_B can be obtained.

$$U_B = \frac{2M_{23}U_D}{M_{12}} \tag{9}$$

As evident in (8) and (9), the system can achieve load-independent CV output and ZPA operation.

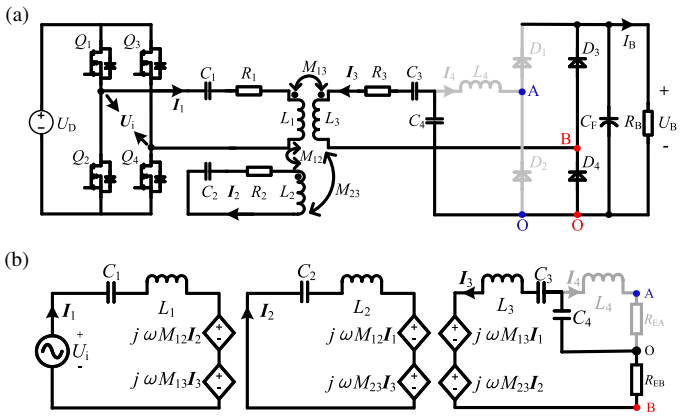

FIGURE 3. The system structure and simplified circuit diagram in CV mode. (a) System structure. (b) Simplified circuit diagram.

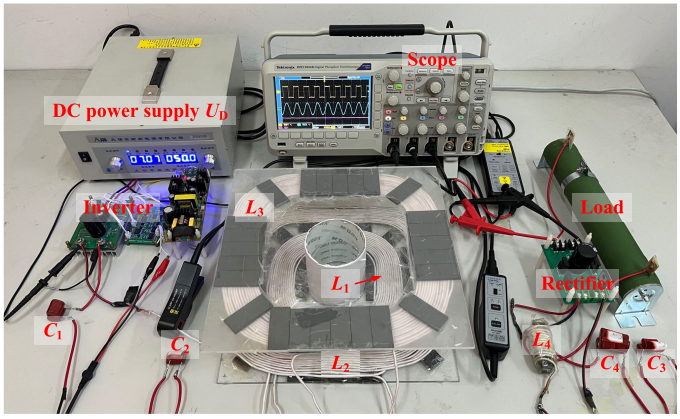

FIGURE 4. Experimental prototype.

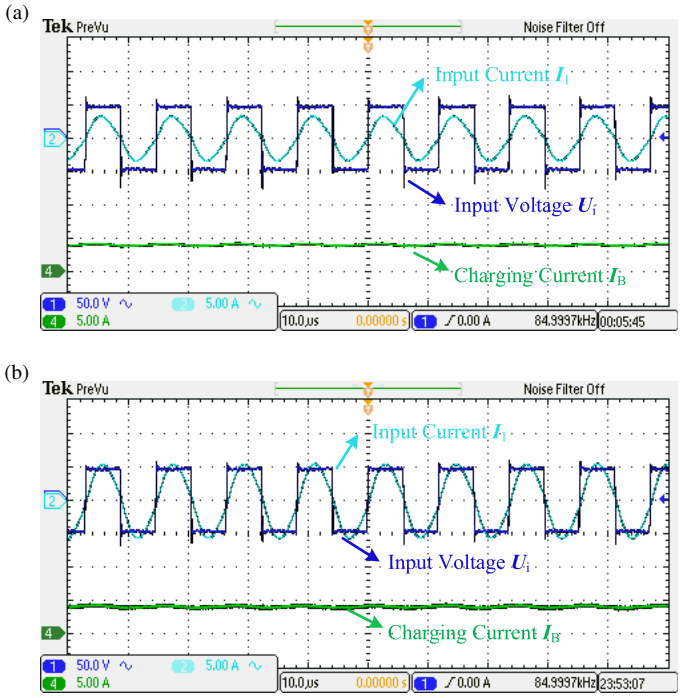

FIGURE 5. Experimental waveforms of $\mathbf{U}_i$, $\mathbf{I}_1$ and I_B in the CC mode when (a) $R_B = 5\,\Omega$ and (b) $R_B = 10\,\Omega$.

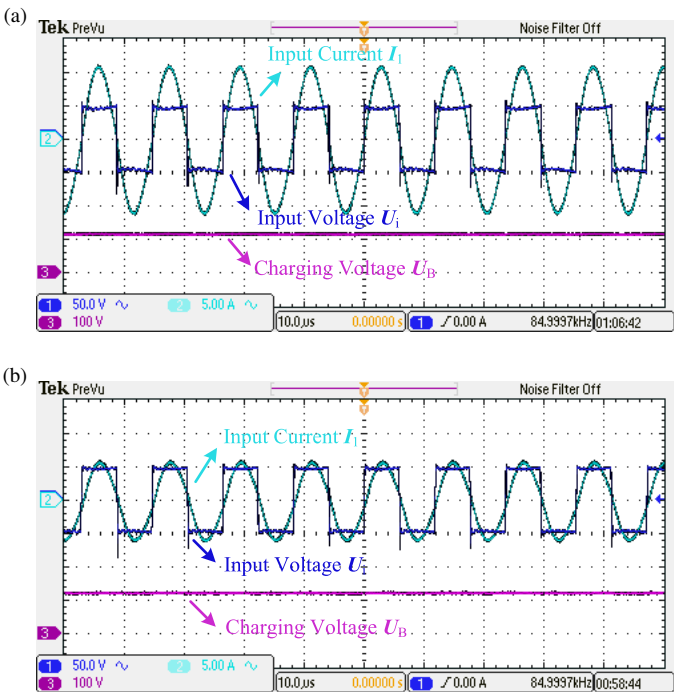

FIGURE 6. Experimental waveforms of $\mathbf{U}_i$, $\mathbf{I}_1$ and U_B in the CV mode when (a) $R_B = 45\,\Omega$ and (b) $R_B = 90\,\Omega$.

3. EXPERIMENTAL VERIFICATION

In order to verify the correctness of the above theoretical analysis, an experimental prototype is fabricated, as displayed in Fig. 4. By combining Equations (3), (6), and (9), the specific parameters of the compensation components in the system can be calculated, as presented in Table 1.

Figure 5 shows the output waveforms of the system when the battery load R_B is $5\,\Omega$ and $10\,\Omega$, respectively. It can be noted that when R_B changes, the charging current I_B is roughly maintained at a constant value of 4 A, which proves that the system has CC output characteristic. Fig. 6 shows the output waveforms of the system when the battery load is $45\,\Omega$ and $90\,\Omega$, respectively. From Fig. 6, it can be found that the system can achieve a stable 120 V CV output. Since the input voltage $\mathbf{U}_i$ and input current $\mathbf{I}_1$ are always in the same phase during the whole charging process, the system can realize ZPA operation.

The efficiency curve of the proposed system from the DC input to the DC output during the whole charging process is shown in Fig. 7. As can be seen from Fig. 7, in CC mode, the power transfer efficiency of the proposed system first climbs from 88.27% to the peak value of 92.07%, and then drops to 91.23% before entering CV mode. In CV mode, the system efficiency rises from 91.23% to the peak value of 93.8%, then drops to 92.17%. During the entire charging process, the sys-

TABLE 1. Specific parameters of the proposed system.

Parameters	Value	Parameters	Value	Parameters	Value
U_D	50 V	L_3	128 μH	M_{12}	24.55 μH
U_B	120 V	L_4	11.5 μH	M_{13}	14.95 μH
I_B	4 A	C_1	66.15 nF	M_{23}	30.35 μH
f	85 kHz	C_2	35.14 nF	R_1	0.08 Ω
L_1	53.04 μH	C_3	43.02 nF	R_2	0.12 Ω
L_2	99.78 μH	C_4	304.869 nF	R_3	0.14 Ω

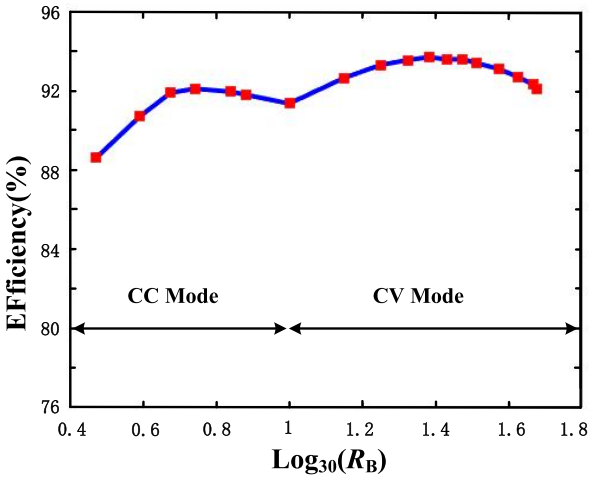

FIGURE 7. Efficiency curve of the proposed system during the entire charging process.

tem efficiency is always maintained at a high level. It is worth noting that the system efficiency in CV mode is high, because the half-bridge rectifier is adopted in CV mode. According to studies in [10, 11], the equivalent AC resistance seen from the half-bridge rectifier is one quarter that of the full-bridge rectifier. Since the load resistance is large in CV mode, the equivalent AC resistance seen from the half-bridge rectifier is closer to the optimal load point, thereby enhancing the efficiency in CV mode.

4. CONCLUSION

This letter proposes a special S-S-LCC compensated three-coil WPT system with CC and CV output characteristics and automatic transition from CC mode to CV mode. In the initial stage of the charging, the CC output can be realized through the S-S-LCC structure. When the battery voltage value rises to exactly equal to the voltage value on the compensation capacitor C_4, the system automatically converts to the S-S-S structure for CV charging. Due to the automatic CC-CV conversion function, the proposed system does not require additional auxiliary circuits, such as wireless communication links, state-of-charge detection circuits, and open circuit protection circuits, etc. Therefore, the proposed system features simple structure, low cost, easy control, and high robustness.

ACKNOWLEDGEMENT

This work was supported in part by Scientific Research Youth Foundation of Hunan Province Education Department of China (No. 22B0803), in part by Natural Science Foundation of Hunan Province (No. 2024JJ7186), in part by Key Laboratory of Small and Micro Intelligent Agricultural Machinery Equipment and Application of Hunan Province Education Department of China (No. SJT012), in part by Institute of Image Information Processing and Intelligent Control of Hunan University of Science and Engineering (No. XKY008).

REFERENCES

[1] Iam, I.-W., I.-U. Hoi, Z. Huang, C. Gong, C.-S. Lam, P.-I. Mak, and R. P. D. S. Martins, "Constant-frequency and noncommunication-based inductive power transfer converter for battery charging," *IEEE Journal of Emerging and Selected Topics in Power Electronics*, Vol. 10, No. 2, 2147–2162, Apr. 2022.

[2] Liu, N. and T. G. Habetler, "Design of a universal inductive charger for multiple electric vehicle models," *IEEE Transactions on Power Electronics*, Vol. 30, No. 11, 6378–6390, Nov. 2015.

[3] Li, H., J. Li, K. Wang, W. Chen, and X. Yang, "A maximum efficiency point tracking control scheme for wireless power transfer systems using magnetic resonant coupling," *IEEE Transactions on Power Electronics*, Vol. 30, No. 7, 3998–4008, Jul. 2015.

[4] Wang, Y., H. Liu, F. Wu, P. Wheeler, Q. Zhou, and S. Zhao, "Research on a three-coil hybrid IPT charger with improved tolerance to coupling variation and load-independent output," *IEEE Journal of Emerging and Selected Topics in Industrial Electronics*, Vol. 4, No. 2, 625–636, Apr. 2023.

[5] Wang, D., X. Qu, Y. Yao, and P. Yang, "Hybrid inductive-power-transfer battery chargers for electric vehicle onboard charging with configurable charging profile," *IEEE Transactions on Intelligent Transportation Systems*, Vol. 22, No. 1, 592–599, Jan. 2021.

[6] Mai, R., Y. Chen, Y. Zhang, N. Yang, G. Cao, and Z. He, "Optimization of the passive components for an S-LCC topology-based WPT system for charging massive electric bicycles," *IEEE Transactions on Industrial Electronics*, Vol. 65, No. 7, 5497–5508, Jul. 2018.

[7] Lu, J., G. Zhu, D. Lin, Y. Zhang, H. Wang, and C. C. Mi, "Realizing constant current and constant voltage outputs and input zero phase angle of wireless power transfer systems with minimum component counts," *IEEE Transactions on Intelligent Transportation Systems*, Vol. 22, No. 1, 600–610, Jan. 2021.

[8] Yang, L., L. Ren, Y. Shi, M. Wang, and Z. Geng, "Analysis and design of an S/S/P-compensated three-coil structure WPT system with constant current and constant voltage output," *IEEE Journal*

of Emerging and Selected Topics in Power Electronics, Vol. 11, No. 3, 2487–2500, Jun. 2023.

[9] Vu, V.-B., D.-H. Tran, and W. Choi, "Implementation of the constant current and constant voltage charge of inductive power transfer systems with the double-sided LCC compensation topology for electric vehicle battery charge applications," *IEEE Transactions on Power Electronics*, Vol. 33, No. 9, 7398–7410, Sep. 2018.

[10] Shu, D. and H. Wang, "Light-load performance enhancement technique for LLC-based PEV charger through circuit reconfiguration," *IEEE Transactions on Transportation Electrification*, Vol. 7, No. 4, 2104–2113, Dec. 2021.

[11] Li, Y., W. Sun, X. Zhu, and J. Hu, "A hybrid modulation control for wireless power transfer systems to improve efficiency under light-load conditions," *IEEE Transactions on Industrial Electronics*, Vol. 69, No. 7, 6870–6880, Jul. 2022.